THE JOURNAL OF BIOLOGICAL CHEMISTRY VOL. 287, NO. 45, pp. 38028–38040, November 2, 2012

Isorhamnetin Inhibits Proliferation and Invasion and Induces Apoptosis through the Modulation of Peroxisome Proliferator-activated Receptor γ Activation Pathway in Gastric Cancer*

Received for publication, June 5, 2012, and in revised form, August 30, 2012 Published, JBC Papers in Press, September 19, 2012, DOI 10.1074/jbc.M112.388702

Lalitha Ramachandran,[a] Kanjoormana Aryan Manu,[a] Muthu K. Shanmugam,[a] Feng Li,[a] Kodappully Sivaraman Siveen,[a] Shireen Vali,[b,c] Shweta Kapoor,[b,c] Taher Abbasi,[b,c] Rohit Surana,[a,d] Duane T. Smoot,[e] Hassan Ashktorab,[e] Patrick Tan,[d,f,g] Kwang Seok Ahn,[h] Chun Wei Yap,[i] Alan Prem Kumar,[a,d,j,k1] and Gautam Sethi[a,d2]

From the [a]Department of Pharmacology, Yong Loo Lin School of Medicine, National University of Singapore, Singapore 117597, [b]Cellworks Group Inc., Saratoga, California, 95070, [c]Cellworks Research India Pvt. Ltd., Bangalore, Karnataka, India, the [d]Cancer Science Institute of Singapore, Centre for Translational Medicine, Singapore 117599, the [e]Department of Medicine and Cancer Center, Howard University, Washington, D. C. 20060, the [f]Genome Institute of Singapore, Singapore 138672, [g]Cancer and Stem Cell Biology, Duke-National University of Singapore Graduate Medical School, Singapore 169857, the [h]College of Oriental Medicine, Kyung Hee University, Seoul 130-701, Republic of Korea, the [i]Pharmaceutical Data Exploration Laboratory, Department of Pharmacy, National University of Singapore, 117543 Singapore, the [j]School of Biomedical Sciences, Faculty of Health Sciences, Curtin University, Perth, Western Australia 6845, Australia, and the [k]Department of Biological Sciences, University of North Texas, Denton, Texas 76203

Background: PPAR-γ, a nuclear transcription factor, plays a critical role in the development of gastric cancer (GC). Hence, novel agents that can modulate PPAR-γ cascade have a great potential for the treatment of GC.
Results: Isorhamnetin (IH) modulates PPAR-γ pathway in GC.
Conclusion: IH induces apoptosis through the activation of the PPAR-γ pathway.
Significance: The study proposes a novel agent for GC treatment.

Gastric cancer (GC) is a lethal malignancy and the second most common cause of cancer-related deaths. Although treatment options such as chemotherapy, radiotherapy, and surgery have led to a decline in the mortality rate due to GC, chemoresistance remains as one of the major causes for poor prognosis and high recurrence rate. In this study, we investigated the potential effects of isorhamnetin (IH), a 3′-*O*-methylated metabolite of quercetin on the peroxisome proliferator-activated receptor γ (PPAR-γ) signaling cascade using proteomics technology platform, GC cell lines, and xenograft mice model. We observed that IH exerted a strong antiproliferative effect and increased cytotoxicity in combination with chemotherapeutic drugs. IH also inhibited the migratory/invasive properties of GC cells, which could be reversed in the presence of PPAR-γ inhibitor. We found that IH increased PPAR-γ activity and modulated the expression of PPAR-γ regulated genes in GC cells. Also, the increase in PPAR-γ activity was reversed in the presence of PPAR-γ-specific inhibitor and a mutated PPAR-γ dominant negative plasmid, supporting our hypothesis that IH can act as a ligand of PPAR-γ. Using molecular docking analysis, we demonstrate that IH formed interactions with seven polar residues and six nonpolar residues within the ligand-binding pocket of PPAR-γ that are reported to be critical for its activity and could competitively bind to PPAR-γ. IH significantly increased the expression of PPAR-γ in tumor tissues obtained from xenograft model of GC. Overall, our findings clearly indicate that antitumor effects of IH may be mediated through modulation of the PPAR-γ activation pathway in GC.

Despite major advances in treatment modalities, gastric cancer (GC)[3] remains the fourth most common cancer in the world and the second cause of cancer-related mortality worldwide (1, 2). Several factors including *Helicobacter pylori* infection, diet, tobacco use, obesity, and genetic alterations have been linked to the onset of gastric cancer (3). Existing treatment strategies include surgery, chemotherapy, and molecular-targeted therapy but are limited by tumor recurrence and chemoresistance (4). Even though GC has been considered as a chemosensitive

* This work was supported by NUS Academic Research Fund Grant R-184-000-170-112 (to G. S.), National Medical Research Council of Singapore Grant R-184-000-211-213, National Medical Research Council of Singapore Grant R-713-000-124-213 (to A. P. K.), and Cancer Science Institute of Singapore, Experimental Therapeutics I Program Grant R-713-001-011-271 (to A. P. K.).

[1] To whom correspondence may be addressed: Cancer Science Inst. of Singapore, National University of Singapore, Centre for Translational Medicine, Singapore 117599. Tel.: 65-65165456; Fax: 65-68739664; E-mail: csiapk@nus.edu.sg.

[2] To whom correspondence may be addressed: Dept. of Pharmacology, Yong Loo Lin School of Medicine, National University of Singapore, Singapore 117597. Tel.: 65-65163267; Fax: 65-68737690; E-mail: phcgs@nus.edu.sg.

[3] The abbreviations used are: GC, gastric cancer; 15d-PGJ2, 15-deoxy-Δ12,14-prostaglandin J2; PPRE, peroxisome proliferator response element; PI, propidium iodide; MTT, 3-(4,5-dimethylthiazol-2-yl)-2,5-diphenyltetrazolium bromide; Bcl-2, B cell lymphoma-2; Bcl-xL, B-cell lymphoma-extra large; CD31, cluster of differentiation 31; LBD, ligand-binding domain; CXCR4, CXC chemokine receptor type 4; PARP, poly(ADP-ribose) polymerase; IH, isorhamnetin; PPAR, peroxisome proliferator-activated receptor.

tumor for many years, no significant progress in its management has resulted within the last two decades with only a few patients experiencing complete pathologic responses to chemotherapy (5, 6). Hence, novel approaches to enhance the effects of chemotherapeutic drugs and improve the existing standard of care are urgently needed.

Peroxisome proliferator-activated receptors (PPARs) are ligand-activated transcription factors that were first discovered 20 years ago (7). There are three isoforms of PPAR; PPAR-α, PPAR-β/δ (also known as PPAR-β or PPAR-δ), and PPAR-γ (8). These have been found in all the mammalian species that have been examined to date (9, 10). PPAR-γ is highly expressed in cancer cells, and treatment with PPAR-γ ligands can induce cell differentiation and apoptosis (11–13). Existing endogenous ligands for PPAR-γ include polyunsaturated fatty acids and the eicosanoids 15-deoxy-Δ12,14-prostaglandin J2 (15d-PGJ2), 13-hydroxyoctadecadienoic acid, and 15-hydroxyeicosatetraenoic acid (14, 15). Detailed analysis by cancer researchers has revealed that PPAR-γ is overexpressed in patients with gastric carcinoma (16). The same study also suggested that PPAR-γ might be a molecular marker for the development of gastric cancer from chronic gastritis. Other studies have shown that PPAR-γ plays a protective role in gastric carcinogenesis and that activation of the receptor has a chemopreventive effect (17). PPAR initiates transcription by heterodimerization with a member of the retinoid X receptor family (18). This is succeeded by binding to a peroxisome proliferator response element (PPRE) within the regulatory region of target genes, which leads to transcriptional activation or repression (19, 20). Although it remains unclear whether PPARs are oncogenes or tumor suppressors, research has also been focused on this receptor because of its involvement in various metabolic disorders that are known to be associated with cancer risk (21–23).

Flavonoids are nonessential dietary factors that are abundantly present in fruits, vegetables, seeds, nuts, tea, and red wine. Many herbs containing flavonoids have been used as traditional medicine (24–26). Quercetin is one such bioflavonoid, known to have several biological effects, including anti-inflammatory and antitumor effects in malignant cancer cells (27). Recent studies have shown that quercetin could alter the morphology and induce apoptosis of gastric cancer cells (28). Isorhamnetin (IH), an immediate metabolite of quercetin, also called 3′-*O*-methylquercetin, has been under attention for its anti-inflammatory and antiproliferative properties in a number of cancers, including colorectal, skin, and lung cancers (29–31). Prior studies have focused on quercetin as an anticancer agent, but recent research has shown that isorhamnetin can induce higher cytotoxicity in tumor cells as compared with quercetin (29). For example, it was found that aflatoxin B1-mediated ROS was inhibited significantly by isorhamnetin when compared with quercetin in hepatocellular carcinoma cells (32).

Because of the critical role of PPAR-γ in GC proliferation, survival, invasion, and metastasis, we investigated whether IH can mediate its antiproliferative and pro-apoptotic effects in GC cells and xenograft model through the activation of the PPAR-γ signaling cascade. Alongside testing the effects of IH in GC cells and xenograft mouse model, we also tested the hypothesis of PPAR-γ activation in a virtual predictive tumor cell system to explore whether IH is mediating its effects primarily through PPAR-γ activation. The predictive epithelial tumor cell platform has been employed to get an insight into how a particular drug individually, or in combination, impacts various cancer phenotypes across different tumor profiles. Thus, our novel approach of combining predictive virtual testing with guided experimental validations is helpful in understanding the mechanism of action and efficacy of novel compounds on physiological end points.

EXPERIMENTAL PROCEDURES

Reagents—RPMI 1640, DMEM and antibiotic-antimycotic mixture were obtained from Invitrogen. Trypsin EDTA, propidium iodide (PI), thiazolyl blue tetrazolium bromide (MTT), crystal violet, isorhamnetin (IH) with chemical structure shown in Fig. 1*A* (>90% purity), 5-fluorouracil, doxorubicin, and β-actin antibody were purchased from Sigma-Aldrich. GSK0660 and GW0742 were purchased from Tocris Bioscience (Ellisville, MO). 15d-PGJ2 and GW9662 were obtained from Cayman (Michigan). FBS was purchased from BioWest (Miami, FL). Capecitabine was obtained from Duheng International Trading Company Ltd. (Shanghai, China). Antibodies against Bcl-2, Bcl-xL, Cyclin-D1, PARP, PPAR-γ, caspase-9/3, and annexin V-FITC assay kit were obtained from Santa Cruz Biotechnology (Santa Cruz, CA). CD31 antibody was purchased from Cell Signaling Technology (Danvers, MA).

Cell Lines—Human GC cell line (AGS) was kindly provided by Prof. Patrick Tan (Duke-NUS Graduate Medical School, Singapore). SNU5 cells were obtained from American Type Culture Collection (Manassas, VA). MKN45 cells were obtained from the Japanese Collection of Research Bioresources. HFE-145 normal gastric epithelial cells were kindly provided by Dr. Hassan Ashktorab (Howard University Cancer Center, Washington, D. C.). AGS cells were cultured in DMEM supplemented with 10% FBS. SNU5, MKN45, and HFE-145 were cultured in RPMI 1640 media supplemented with 10% FBS. The cells were maintained at 37 °C in an atmosphere of 5% CO_2, 95% air.

MTT Assay—The antiproliferative effect of IH against various GC cells was determined by the MTT dye uptake method. Briefly, the cells (5×10^3/well) were incubated in triplicate in a 96-well plate in the presence or absence of indicated concentrations of IH in a final volume of 0.2 ml for different time intervals at 37 °C. Thereafter, 20 ml of MTT solution (5 mg/ml in PBS) was added to each well. After a 4-h incubation in the dark at 37 °C, 0.1 ml of lysis buffer (20% SDS, 50% dimethylformamide) was added and incubated for 2 h at 37 °C, followed by measurement of optical density at 570 nm by Tecan plate reader (Durham, NC).

Molecular Docking Analysis—An x-ray crystallography structure of PPAR-γ (Protein Data Bank code 2Q5S) was obtained from the RCSB Protein Data Bank. This structure was selected because it has a relatively good resolution of 2.05 Å, with an *R* value of 0.199 and an R_{free} value of 0.245. The protein file contains two copies of PPAR-γ. The first copy, chain A was removed because it contains less residues than the second copy, chain B. The ligand associated with chain A and all water molecules were also removed. The remaining protein chain and its

associated ligand were then processed using the default settings for the Protonate 3D feature in the software molecular operating environment to add hydrogen atoms and determine the ionization state of the residues. Molecular docking of IH to PPAR-γ was then performed using the Dock feature in the molecular operating environment. The Alpha PMI algorithm was used to generate 250 different poses for IH. Alpha HB scoring function was used to rank these poses. The top 10 poses were retained and further refined by energy minimization. The MMFF94x force field using the Reaction Field model was used for the energy minimization. Side chains of residues with 6 Å from the ligand were allowed to move during energy minimization. After energy minimization, the pose with the best interaction energy with the receptor was retained, as described previously (33).

PPAR-γ Competitive Binding Assay—A binding assay was performed to test whether IH could competitively bind to PPAR-γ using LanthaScreen™ time-resolved FRET PPAR-γ competitive binding assay kit (Invitrogen). A terbium-labeled anti-GST antibody was used to indirectly label a nuclear receptor by binding to its GST tag. When a fluorescent ligand (tracer) binds to the receptor, energy transfer from the antibody to the tracer occurs, and a high time-resolved FRET ratio is observed. Competitive ligand binding to the nuclear receptor is detected by the ability of a test compound to displace the tracer from the nuclear receptor, which results in a loss of FRET signal between the antibody and the tracer. The assay was performed with various concentrations of IH as described in figure legends. The curve was plotted using a sigmoidal dose-response equation with varying slope using Prism® software from GraphPad™ Software, Inc.

Flow Cytometric Analysis—To determine the effect of IH on the cell cycle, GC cells were first seeded at a density of 2×10^5 cells/well in a 6-well titer plate and incubated at 37 °C overnight. They were then exposed to IH for the various time intervals as described in the figure legends. Thereafter cells were washed, fixed with 70% ethanol, and incubated for 30 min at 37 °C with 0.1% RNase-A in PBS. The cells were then washed again, resuspended, and stained in PBS containing 25 μg/ml PI for 30 min at room temperature. Cell distribution across the cell cycle was analyzed with a CyAn ADP flow cytometer (Dako Cytomation) as described previously (34).

Annexin V Assay—GC cells were first seeded at a density of 2×10^5 cells/well in a 6-well titer plate and allowed to incubate at 37 °C overnight. After treatment with IH for the indicated time intervals, cells were trypsinized, washed with binding buffer, and resuspended in annexin V-FITC-added binding buffer for 15 min under dark conditions and washed and stained with PI-containing binding buffer. The samples were then analyzed immediately by flow cytometry as described previously (34).

Wound Healing Assay—The migration of cells was investigated using a wound healing assay. GC cells were seeded in a 6-well microtiter plate until ~80% confluent. A wound was created using a pipette tip and each well was rinsed with PBS to remove detached cells. The cells were pretreated with GW9662, a pharmacological PPAR-γ specific inhibitor for 2 h, followed by incubation with IH for 8 h. The microscopic observation of the cells was recorded as described previously (35).

Invasion Assay—The BD BioCoat Tumor Invasion system is a chamber that has a light-tight polyethylene terephthalate membrane with 8-μm diameter pores and is coated with a reconstituted basement membrane gel (BD Biosciences). 2×10^5 GC cells were suspended in serum-free DMEM and seeded into the Matrigel Transwell chambers. The cells were pretreated with GW9662, a pharmacological PPAR-γ specific inhibitor for 2 h, followed by incubation with IH for 8 h. After incubation, the outer surfaces of the Transwell chambers were wiped with cotton swabs, and the invading cells were fixed and stained with crystal violet solution. The invading cells were then counted in five randomly selected areas under microscopic observation as described previously (35).

Luciferase Assay—The activity of PPAR-γ was investigated using luciferase assay as described previously (36). Firstly, GC cells were seeded at density of 5×10^4 cells/well in a 12-well microtiter plate followed by overnight incubation. The cells were incubated in serum-free DMEM for at least 1 h before transfection with pPPRE-tk-Luc (three PPREs from rat acyl-CoA oxidase promoter under the control of the herpes simplex virus thymidine kinase promoter). For PPARs study, the cells were transfected with each of GAL4-PPAR-α LBD, GAL4-PPAR-β LBD, and GAL4-PPAR-γ LBD plasmids (a generous gift from Dr. Javier F. Piedrafita, Torrey Pines Institute for Molecular Studies, San Diego, CA), together with GAL4-Luc. For dominant negative transfection, the cells were transfected with PPAR-γ mutant or pCMX-PPAR-γ plasmid (a cDNA clone encoding the mouse PPAR-γ; a generous gift from Dr. Ronald M. Evans, The Salk Institute for Biological Studies, San Diego, CA), together with pPPRE-tk-Luc. The cells were lysed in reporter lysis buffer, and luciferase activity was measured with a Tecan (Durham, NC) plate reader and normalized against β-galactosidase activity.

Western Blot Analysis—For detection of various proteins, GC cells were first seeded at a density of 3×10^5 cells/well on a 6-well micro-titer plate and treated with IH for different time intervals. The cells were then washed with 1× PBS and incubated on ice for 30 min in 0.05 ml of lysis buffer (2.0 mM Tris, pH 7.4, 2.50 mM NaCl, 2 mM EDTA, pH 8.0, 0.1% Triton X-100, 0.01 mg/ml aprotinin, 0.005 mg/ml leupeptin, 0.4 mM PMSF, and 4 mM Na_3VO_4). The lysate was then centrifuged at 12,000 rpm for 3 min to remove the cell debris, after which the supernatant was collected. Whole cell extract protein (ranging from 30 to 70 μg) was resolved on 12%, 10%, and 15% SDS-PAGE depending on the size of protein of interest, electrotransferred onto a nitrocellulose membrane, blocked (Blocking One, Nacalai USA, Inc.) for 60 min, and blotted with antibodies against Bcl-2, Bcl-xL, Cyclin-D1, PPAR-γ, procaspase-3, procaspase-9, and PARP and then detected by chemiluminescence (ECL; GE Healthcare, Little Chalfont, UK).

RNA Extraction and Real Time PCR Analysis—Total RNA was extracted using the TRIzol reagent (Invitrogen), according to the manufacturer's instructions. Reverse transcription was then carried out as described previously (34). Briefly, for a 50-μl reaction, 10 μl of RT product was mixed with 1× Taq-Man® Universal PCR Master mix, 2.5 μl of 20× TaqMan probes for Bcl-2, Bcl-xL, and cyclin D1, respectively, 2.5 μl of 20 × 18 S RNA TaqMan probe as the endogenous control for each target-

ing gene and topped up to 50 μl with sterile water. A negative control for RT, in which sterile water replaced the RNA template, was included. Another control, where RT mix was replaced with sterile water, was included to check for DNA contamination. Real time PCR was done using the 7500 Fast Real-Time PCR System (ABI PRISM 7500; Applied Biosystems, Foster City, CA) with the following protocol: 50 °C for 2 min, 95 °C for 10 min, followed by 40 cycles of denaturing at 95 °C for 15 s and extension at 60 °C for 1 min. The results were analyzed using Sequence Detection Software version 1.3 provided by Applied Biosystems. Relative gene expression was obtained after normalization with endogenous human GAPDH and determination of the difference in threshold cycle (C_t) between treated and untreated cells using the $2 - \Delta\Delta C_t$ method. Primers and probes for human Bcl-2, Bcl-xL, and cyclin D1 were purchased as kits from Applied Biosystems (Assays-on-Demand).

Virtual Predictive Studies—Predictive analysis was performed using virtual tumor cell technology (Cellworks Group Inc., Saratoga, CA), which has been extensively validated and aligned with cancer physiology (34). The Cellworks tumor cell platform provides a dynamic and transparent view of cancer disease cellular physiology at the functional proteomics abstraction level. The open-access architecture of the platform provides a framework for different "what if" analysis and studies in an automated high-throughput methodology. The Cellworks platform is implemented using a three-layered architecture. The top later is a text user interface/graphic user interface. The middle layer is the comprehensive representation of signaling and metabolic pathways covering all cancer phenotypes. The bottom layer is the computational backplane, which enables the system to be dynamic and computes all the mathematics in the middle layer.

Platform Description—The virtual tumor cell platform consists of a dynamic and kinetic representation of the signaling pathways underlying tumor physiology at the biomolecular level. All the key relevant protein players and associated gene and mRNA species with regard to tumor-related signaling are comprehensively included in the system with their relationship quantitatively represented. Pathways and signaling for different cancer phenotypes comprise 20000 plus cross-talk with more than 8000 intracellular molecules. The platform includes important signaling pathways comprising growth factors like EGF receptor, PDGF receptor, α polypeptide, FGF receptor, c-MET, VEGF receptor, and insulin-like growth factor 1 receptor; cell cycle regulators; mammalian target of rapamycin signaling; p53 signaling cascade, cytokine pathways like IL1, IL4, IL6, IL12, and TNF; lipid mediators; and tumor metabolism. Fig. 1*B* shows the customized Cellworks tumor cell platform that was created to align to the AGS human gastric cancer cell line (kirsten rat sarcoma viral oncogene homolog mutant, PI3K catalytic subunit mutant, runt-related transcription factor 3 deleted, β-catenin mutant, and cadherin 1 deleted).

Predictive Study Experimental Protocol—The virtual tumor cell is simulated in the proprietary Cellworks computational backplane and initialized to a control state wherein all molecules attain the control steady state values, following which the triggers are introduced into the system. The virtual tumor cell technology allows the end user to align the system to a known cancer cell line with perturbations in known markers or mutations that can be used for further analysis (35). In this kinetic based virtual tumor cell platform, there is no statistical variation in the outputs. The system provides predictive semiquantitative trends visibility into all phenotypes and biomarkers. The system predictions have been validated against a large number of retrospective and prospective studies, and the accuracy of predictions is very high.

Xenograft Tumor Model—All of the procedures involving animals were reviewed and approved by NUS Institutional Animal Care and Use Committee. Six-week-old athymic nu/nu female mice (Biological Resource Centre, Biopolis, Singapore) were implanted subcutaneously in the right flank with SNU-5 cells (3×10^6 cells/100 μl of saline). When tumors have reached 0.25 cm in diameter, the mice were randomized into the following treatment groups ($n = 5$/group): (*a*) untreated control (corn oil, 100 μl daily) and (*b*) IH (1 mg/kg of body weight, suspended in corn oil, intraperitoneal injection) thrice/week. Therapy was continued for 4 weeks, and the animals were euthanized 1 week later. Tumor tissues were thereafter fixed in formalin and embedded in paraffin for immunohistochemistry and routine hematoxylin and eosin staining.

Immunohistochemical Analysis of Tumor Tissues—Solid tumors from control and IH treated groups were fixed with 10% phosphate-buffered formalin, processed, and embedded in paraffin. The sections were cut, deparafinized in xylene, dehydrated in graded alcohol, and finally hydrated in water. Antigen retrieval was performed by boiling the slide in 10 mM sodium citrate, pH 6.0, for 30 min. Immunohistochemistry was performed following manufacturer instructions (DAKO LSAB kit). Briefly, endogenous peroxidases were quenched with 3% hydrogen peroxide. Nonspecific binding was blocked by incubation in the blocking reagent in the LSAB kit (Dako, Carpinteria, CA) according to the manufacturer's instructions. Sections were incubated overnight with primary antibodies as follows: anti-PPAR-γ, anti-Bcl-2, and anti-CD31 (each at 1:100 dilutions). The slides were subsequently washed several times in Tris-buffered saline with 0.1% Tween 20 and were incubated with biotinylated linker for 30 min, followed by incubation with streptavidin conjugate provided in LSAB kit according to the manufacturer's instructions. Immunoreactive species were detected using 3,3-diaminobenzidine tetrahydrochloride as a substrate. The sections were counterstained with Gill's hematoxylin and mounted under glass coverslips. Images were taken using an Olympus BX51 microscope (magnification, 20×). Positive cells (brown) were quantitated using the Image-Pro plus 6.0 software package (Media Cybernetics, Inc.).

Statistical Analysis—The data has been represented in bar graph format expressed as the means ± S.E. from at least two independent experiments. Statistical analysis was performed by Student's *t* test and one-way analysis of variance. A *p* value of less than 0.05 (*, $p < 0.05$; **, $p < 0.01$) was considered statistically significant.

RESULTS

Predictive Proteomics Analysis for the Effect of IH on GC Cells—Using the virtual epithelial tumor cell platform, predictive proteomics studies were conducted, and IH was represented to be

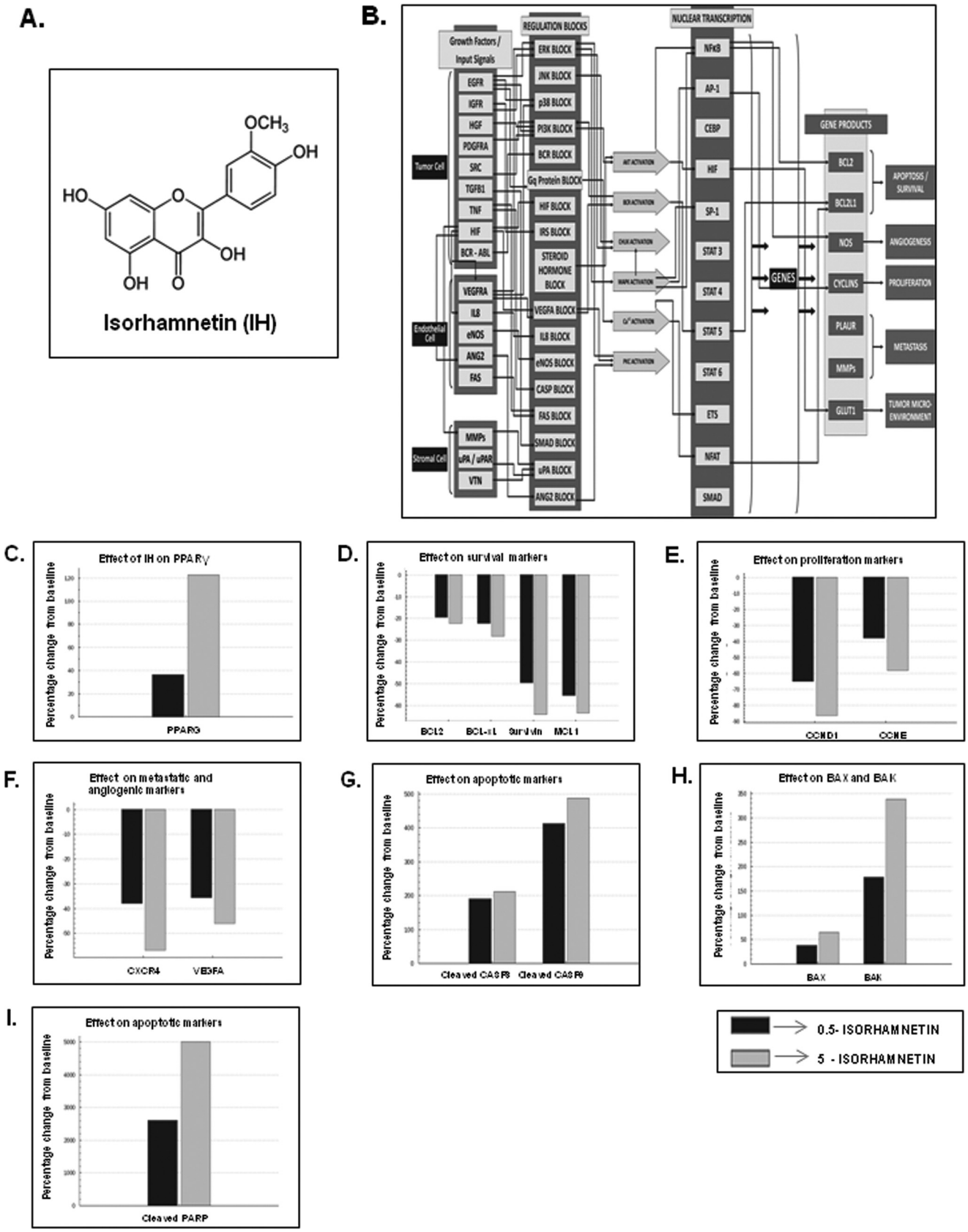
A.
Isorhamnetin (IH)
B.
Growth Factors / Input Signals
EGFR
IGFR
HGF
PDGFRA
SRC
TGFB1
TNF
HIF
BCR - ABL
VEGFRA
IL8
eNOS
ANG2
FAS
MMPs
uPA / uPAR
VTN
Tumor Cell
Endothelial Cell
Stromal Cell
REGULATION BLOCKS
ERK BLOCK
JNK BLOCK
p38 BLOCK
PI3K BLOCK
BCR BLOCK
Gq Protein BLOCK
HIF BLOCK
IRS BLOCK
STEROID HORMONE BLOCK
VEGFA BLOCK
IL8 BLOCK
eNOS BLOCK
CASP BLOCK
FAS BLOCK
SMAD BLOCK
uPA BLOCK
ANG2 BLOCK
NUCLEAR TRANSCRIPTION
NFκB
AP-1
CEBP
HIF
SP-1
STAT 3
STAT 4
STAT 5
STAT 6
ETS
NFAT
SMAD
GENES
GENE PRODUCTS
BCL2
BCL2L1
NOS
CYCLINS
PLAUR
MMPs
GLUT1
APOPTOSIS / SURVIVAL
ANGIOGENESIS
PROLIFERATION
METASTASIS
TUMOR MICRO-ENVIRONMENT
C.
Effect of IH on PPARγ
Percentage change from baseline
PPARG
D.
Effect on survival markers
Percentage change from baseline
BCL2
BCL-xL
Survivin
MCL1
E.
Effect on proliferation markers
Percentage change from baseline
CCND1
CCNE
F.
Effect on metastatic and angiogenic markers
Percentage change from baseline
CXCR4
VEGFA
G.
Effect on apoptotic markers
Percentage change from baseline
Cleaved CASP8
Cleaved CASP9
H.
Effect on BAX and BAK
Percentage change from baseline
BAX
BAK
I.
Effect on apoptotic markers
Percentage change from baseline
Cleaved PARP
0.5- ISORHAMNETIN
5 - ISORHAMNETIN

an activator of PPAR-γ at tested concentrations of 0.5 and 5 μM with a K_a of 1.19 μM (Fig. 1*C*). Interestingly, investigation of the effects of IH on antiapoptotic genes such as Bcl-2, Bcl-xL, survivin, and Mcl1 showed a positive correlation with IH down-regulating the expression of all four genes (Fig. 1*D*). Of the two proliferative markers tested, Cyclin D1 was found to show a higher reduction as compared with Cyclin E on treatment with IH (Fig. 1*E*). The impact of IH on angiogenic and metastatic markers VEGFA and CXCR4 was also studied, and a reduction of ~55 and 45% with 5 μM of IH, respectively, was observed in both these markers (Fig. 1*F*). Caspases-9 and -3 were found to increase on treatment with IH (Fig. 1*G*). Of the apoptotic gene products, Bak showed a higher increase when compared with Bax (Fig. 1*H*). Cleaved PARP1 was found to show a very high increase of ~250 and ~500% with 0.5 and 5 μM of IH (Fig. 1*I*).

IH Suppresses the Proliferation of GC Cell Lines and Enhances the Apoptotic Effects of Chemotherapeutic Agents—The antiproliferative effect of IH was investigated in three GC cell lines using the MTT assay. The cells were treated for 12, 24, and 48 h with 0, 10, 25, and 50 μM concentrations of IH. IH was found to significantly inhibit the proliferation of all three GC cells in a dose- and time-dependent manner. Of the three GC cell lines, AGS was found to be most sensitive to antiproliferative effects of IH and hence selected for detailed mechanistic studies (Fig. 2*A*). Interestingly, we observed that IH had minimal effect on the proliferation of normal gastric epithelial HFE-145 cells. Next we examined using MTT assay whether IH at suboptimal concentration could enhance the cytotoxic effects of chemotherapeutic agents commonly employed for GC treatment. Growth inhibition rate was obtained and calculated as the percentage of dead cells *versus* control. Following a 24-h treatment, it was found that IH could enhance the cytotoxicity of three chemotherapeutic agents; namely, doxorubicin, capecitabine, and 5-fluorouracil (Fig. 2*B*). 10 μM of IH was found to enhance the cytotoxic activity of 5-fluorouracil, doxorubicin, and capecitabine by 1.63-, 1.89-, and 1.4-fold, respectively. These results support the predictive analysis seen with inhibition of proliferation markers as reported in Fig. 1*E*.

IH Causes the Accumulation of GC Cells in the Sub-G1 Phase, Decreases Expression of Antiapoptotic Proteins, and Induces PARP Cleavage—To investigate whether IH could induce apoptosis in GC cells, cell cycle distribution after PI staining was analyzed. The cells were treated with 25 μM IH for 0, 12, 24, and 48 h. Our analysis showed that IH caused increased accumulation of the cell population in the sub-G1 phase in a time-dependent manner (Fig. 2*C*). Under similar conditions, the expression of another apoptosis marker, phosphatidylserine distribution on the cell membrane was analyzed by flow cytometry with annexin V-FITC staining. The results showed that IH was able to increase annexin V-positive cells in a time-dependent manner, thus indicating induction of early apoptosis (Fig. 2*D*). Whether IH could modulate the expression of various genes involved in GC survival was also determined. We found that IH could down-regulate the expression of antiapoptotic and proliferative proteins such as Bcl-2, Bcl-xL, and Cyclin D1 in a time-dependent manner as observed by Western blot analysis, confirming the predictive results using Cellworks Tumor Cell technology. It was further observed that IH could also down-regulate the protein levels of procaspase-9 and -3 and induce substantial PARP cleavage in GC cells (Fig. 2*E*). The results indicate that IH could induce significant apoptosis in GC cells and clearly correlate with predictive results shown in Fig. 1 (*G* and *I*). To determine whether IH also affects the transcription of these genes, the mRNA expression of Bcl-2, Bcl-xL, and Cyclin D1 was also examined. The mRNA of these genes was constitutively expressed in AGS cells, and treatment with IH suppressed the expression in a time-dependent manner with maximum reduction observed after 4 h of treatment (Fig. 2*F*). These results suggest that IH can modulate the expression levels of various genes involved in proliferation and survival of GC at both protein and mRNA levels.

IH Suppresses Migration and Invasion of GC Cells, and This Property Is Reversed in the Presence of a Pharmacological PPAR-γ-specific Inhibitor—The effect of IH on the migratory potential of GC cells was investigated using the wound healing assay. A wound was created with a pipette tip, and the migration of cells to fill up the wound was recorded by microscopic observation. We found that IH alone significantly suppressed the migration of GC cells, and the pretreatment with GW9662, a pharmacological PPAR-γ inhibitor, reversed the antimigratory effects of IH as shown in Fig. 3*A*.

Also, a BD biocoat tumor invasion system was used to study the effect of IH on invasion of GC cells. Upon treatment with IH, there was a reduction in the number of cells that could invade the chamber, indicating that IH could indeed significantly inhibit the invasive property of GC cells (Fig. 3*B*). Moreover, we found that the pretreatment with GW9662 reversed the anti-invasive potential of IH in GC cells.

IH Induces Activity of PPAR-γ and PPAR-β/δ Activity in GC Cells—A reporter luciferase assay was performed to systematically study the effect of IH on the activity of various PPARs in

FIGURE 1. *A*, the chemical structure of IH. *B*, predictive *in silico* virtual tumor cell platform generated results. The figure illustrates a high level view of the maze of interactions and cross-talks present in the virtual tumor cell platform. The Cellworks virtual epithelial tumor cell platform on which predictive studies were conducted is an integrated representation of the pathways in cancer that includes phenotypes of proliferation, apoptosis, angiogenesis, metastasis, and conditions of tumor microenvironment such as tumor-associated inflammation. The set of graphs here demonstrate the effect on biomarkers upon treatment with IH. IH was shown as a PPAR-γ agonist in the system and tested on the AGS baseline at 0.5 and 5 μM with a K_a of 1.19 μM. *C*, effect on increase in PPAR-γ activity with IH. PPARG shows increases of 1.36- and 2.22-fold, respectively, with 0.5 and 5 μM of IH. *D*, the figure shows the effect of IH on survival markers-Bcl-2, Bcl-xL, survivin, and Mcl-1. Survivin and myeloid cell leukemia sequence 1 (Bcl-2-related) show a higher reduction with IH varying from 50–60% as compared with Bcl-2 and Bcl-xL where we see a reduction of ~20–30%. *E*, the figure depicts the impact of IH on proliferative markers-CCND1 (Cyclin D1) and CCNE (Cyclin E). CCND1 is showing almost a 90% reduction with 5 μM of IH, and CCNE is showing a reduction of 40 and 60%, respectively, at the two dosages for IH. *F*, the figure shows the impact of IH on angiogenic and metastatic markers VEGFA and CXCR4. CXCR4 is showing a reduction of ~38 and ~58% with 0.5 and 5 μM of IH, and VEGFA shows a reduction of 35 and 45%, respectively. *G*, the impact of IH on apoptotic markers: active CASP3 and CASP9. CASP9 is showing a higher increase of 500% with IH treatment as compared with CASP3, which is showing a 200% increase with IH. *H*, the impact of IH on BAX and BAK levels. BAK is showing an increase of 175 and 340% with 0.5 and 5 μM of the drug. The increase in BAX is only ~50%. *I*, the effect of IH on cleaved PARP1. PARP1 cleaved is showing an increase of 2500 and 5000% with 0.5 and 5 μM of IH, respectively.

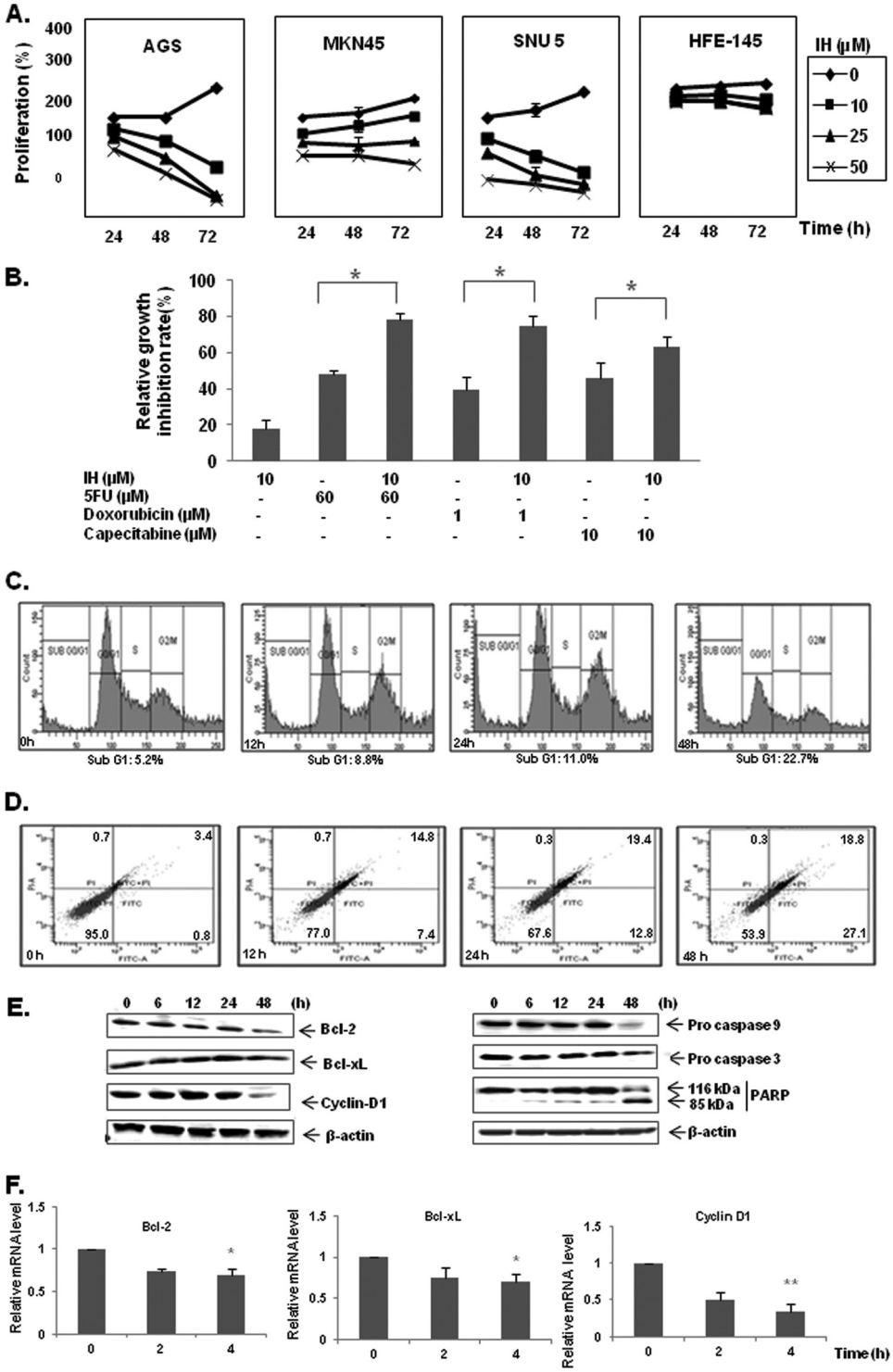

FIGURE 2. *A*, antiproliferative effects of IH in AGS, MKN45, SNU5 gastric cancer cells, and HFE-145 gastric epithelial cells. Cell viability was determined by MTT assay and is reported as the percentage of viable cells relative to the control. The values are the means ± S.E. of three independent experiments. *B*, IH potentiates the effect of various chemotherapeutic drugs (5-fluorouracil, doxorubicin, and capacetabine) in the AGS cell line significantly. AGS cells were treated with either 10 μM IH alone or in combination with various chemotherapeutic drugs for 24 h before MTT solution was added. The data were expressed as the percentages of dead cells relative to the control. The values are the means ± S.E. of three independent experiments. *, $p < 0.05$. *C*, time-dependent effects of IH on cell cycle distribution in AGS cells. The cells were exposed to 25 μM of IH for 12, 24, and 48 h followed by propidium iodide staining. The data are representative of three independent experiments. *D*, IH induces apoptosis in a time-dependent manner as observed by annexin V staining. The data are representative of three independent experiments. *E*, Western blot analysis of various gene products upon IH treatment. AGS cells were treated with 25 μM IH for 6, 12, 24, and 48 h. Whole cell extracts were resolved on SDS-PAGE and probed with the indicated antibodies. The data are representative of at least three independent experiments. *F*, AGS cells were treated with 25 μM IH for the indicated time intervals, after which cells were harvested, and RNA samples were extracted. 1-μg portions of the respective RNA extracts were subjected to reverse transcription to generate corresponding cDNA. Real time PCR was performed to measure the relative quantities of mRNA. Each RT product was targeted against Bcl-2, Bcl-xL, and cyclin D1 TaqMan probes, with HuGAPDH as endogenous control for measurement of equal loading of RNA samples. The results were analyzed using Sequence Detection Software version 1.3 provided by Applied Biosystems. *, $p < 0.05$; **, $p < 0.01$.

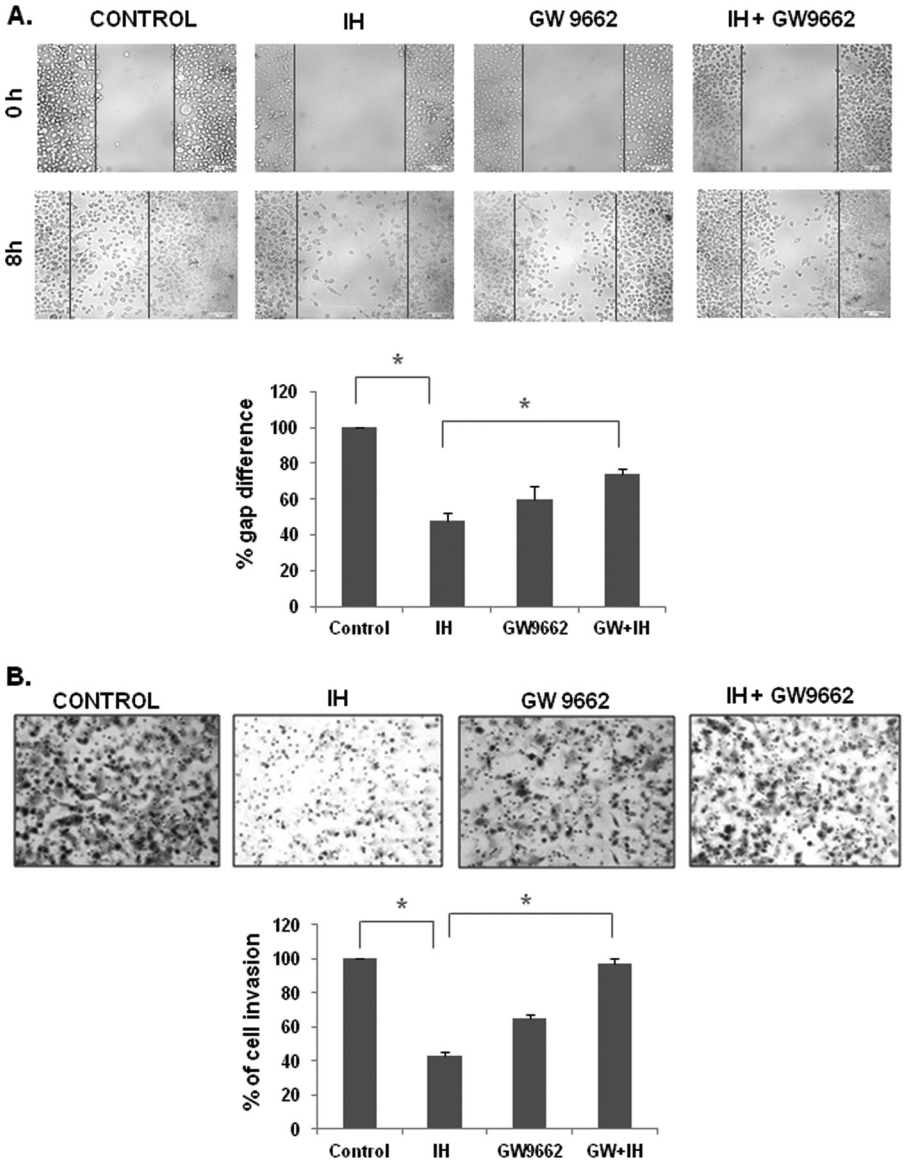

FIGURE 3. *A*, microscopic observation of the migration of AGS cells after pretreatment with GW9662 (20 μM for 2 h), followed by incubation with IH for 8 h. The cells were also treated alone with 25 μM IH for 8 h and GW9662 (20 μM for 2 h). The data are representative of three independent experiments. *B*, the cell invasion assay for evaluating the inhibitory effect of IH on gastric cancer cell invasion after pretreatment with GW9662 (20 μM for 2 h), followed by incubation with IH for 8 h. The cells were also treated alone with 25 μM IH for 8 h and GW9662 (20 μM for 2 h). The cells were fixed with 4% paraformaldehyde before staining with 0.5% crystal violet as described under "Experimental Procedures." The percentage of the migratory cells of the treated group was normalized against the untreated group. The values are the means ± S.E. of two or three independent experiments. *, $p < 0.05$.

gastric cancer cells. The cells were transfected with each of the PPAR plasmids, GAL4-PPAR-γ LBD, and GAL4-PPAR-δ LBD plasmids, together with GAL4-Luc and treated with IH for 18 h. It was found that IH induced the activities of both PPAR-β/δ (Fig. 4*A*, *left panel*) and PPAR-γ (Fig. 4*A*, *right panel*). To examine the specificity of IH on the activity of PPAR-β/δ and PPAR-γ, luciferase assay was performed in the presence of their respective antagonists. It was found that GSK0660, an antagonist of PPAR-β/δ, was unable to reverse IH-induced PPAR-β/δ activity (Fig. 4*B*, *left panel*), whereas similar concentrations of GSK0660 could reverse the effect of GW0472, a pharmacological PPAR-β/δ agonist (Fig. 4*B*, *right panel*), suggesting that the effect of IH on PPAR-β/δ was not specific. However, the antagonist of PPAR-γ, GW9662, could significantly reverse IH-induced PPAR-γ activity (Fig. 4*C*, *left panel*), as well as activity of 15d-PGJ_2, a classical PPAR-γ agonist (Fig. 4*C*, *right panel*), thereby suggesting that the anticancer effects of IH may be mediated through PPAR-γ pathway.

IH Induces PPAR-γ Activity in GC Cells—Because of the specific effect of IH on PPAR-γ activity in GC cells and in view of the fact that PPAR-γ has been extensively shown to be associated with anticancer effects in a variety of cancer types including GC, we choose to focus on this isoform and its potential role in the observed anticancer effects of IH. First, the molecular docking of IH to PPAR-γ using the Dock feature in the molecular operating environment was performed as described under "Experimental Procedures." IH was able to form interactions with seven polar residues and six nonpolar residues in the receptor within the ligand-binding pocket of PPAR-γ that were reported to be critical for its activity (Fig. 5*A*, *left panel*). The

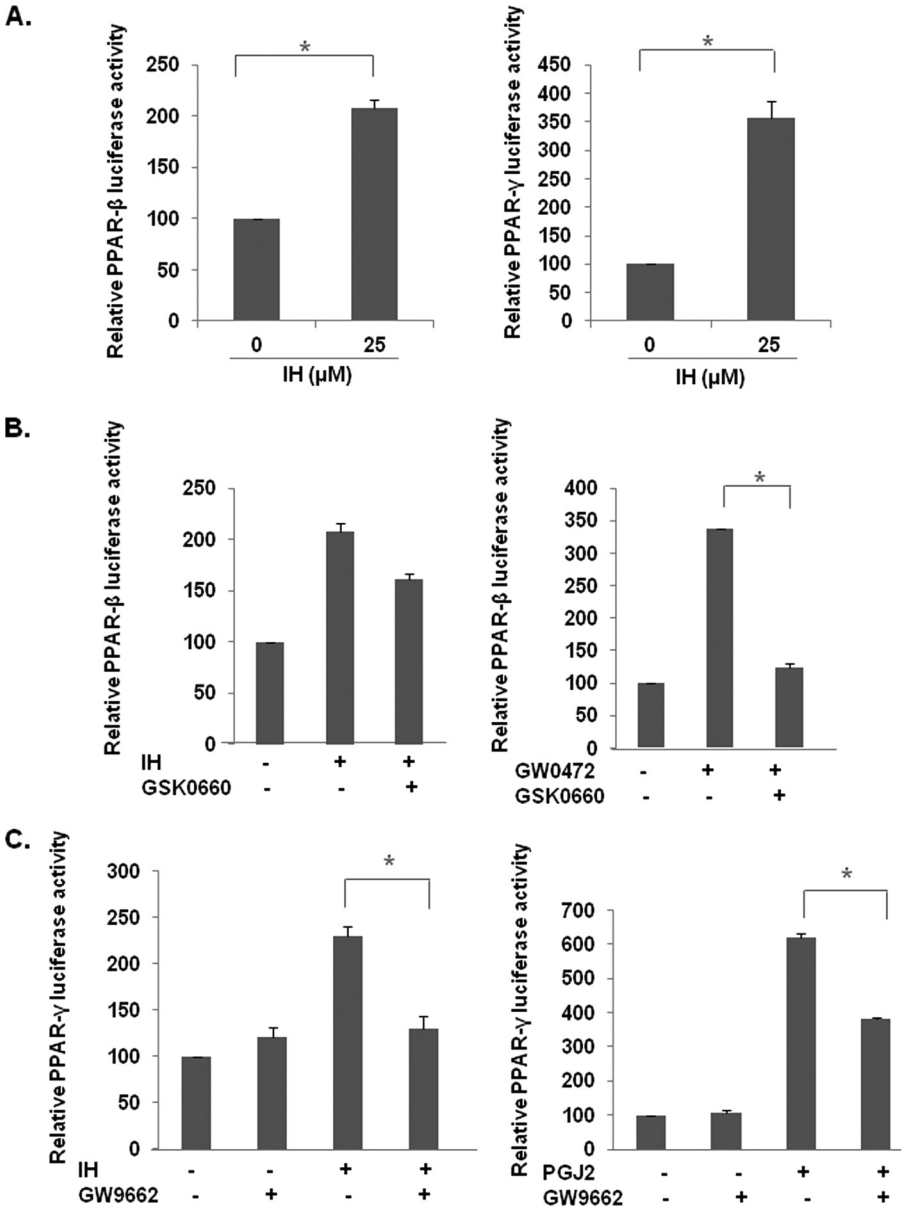

FIGURE 4. **Effect of IH PPAR activity in GC cells.** *A*, effect of IH in PPARs. The cells were transfected with GAL4-PPAR-β/δ LBD and GAL4-PPAR-γ LBD plasmids, together with GAL4-Luc and β-gal plasmids for 4 h before treatment with 25 μM IH for 18 h. The data are expressed as percentages of the respective PPAR activity relative to the control. The values are the means ± S.E. of two or three independent experiments. *, $p < 0.05$. *B*, the inhibitor of PPAR-β/δ, GSK0660, could not block IH-induced PPAR-β/δ activity. The cells were transfected with GAL4-PPAR-β/δ LBD plasmids together with GAL4-Luc and β-gal plasmid for 4 h. The cells were pretreated with 50 μM GSK0660 for 4 h before treatment with 25 μM IH or 10 μM GW0742, a PPAR-β/δ agonist, both for 18 h. The data are expressed as percentages of the PPAR-β/δ activity relative to the control. The values are the means ± S.E. of two or three independent experiments. *, $p < 0.05$. *C*, IH-induced PPAR-γ activity could be blocked by GW9662, an inhibitor of PPAR-γ. The cells were transfected with GAL4-PPAR-γ LBD plasmids together with GAL4-Luc and β-gal plasmid for 4 h. The cells were pretreated with 10 μM or 20 μM GW9662 for 2 h before treatment with 25 μM IH or 20 μM PGJ2, a PPAR-γ agonist, both for 18 h. The data are expressed as percentages of the PPAR-γ activity relative to the control. The values are the means ± S.E. of two or three independent experiments. *, $p < 0.05$.

three-dimensional conformational structure of IH inside PPAR-γ is shown in (Fig. 5*A*, *right panel*). The dose- and time-dependent effect of IH on PPAR-γ activity in GC cells was also determined. AGS cells were pretransfected with pPPRE-tk-Luc and β-gal plasmids, followed by treatment with different concentrations of IH for 8 h. After normalization with the vehicle control, it was found that IH could significantly increase PPAR-γ activity and expression in a dose-dependent manner, with maximum effect at 50 μM concentration (Fig. 5*B*, *left panel*). IH also increased PPAR-γ activity in a time-dependent manner, with maximum activity recorded at 8 h (Fig. 5*B*, *right panel*).

Also, an *in vitro* binding assay was performed to determine whether IH could competitively bind to PPAR-γ. Serial dilutions of IH were prepared in a 384-well polypropylene assay plate. Fluormone™ Pan-PPAR Green, PPAR-γ-LBD, and Tb-anti-GST Ab were then added to each sample well as described in the protocol. The assay mixture was incubated for 1 h at room temperature prior to measuring the 520-nm/490-nm emission ratio of each well. The *error bars* represent the S.E. of

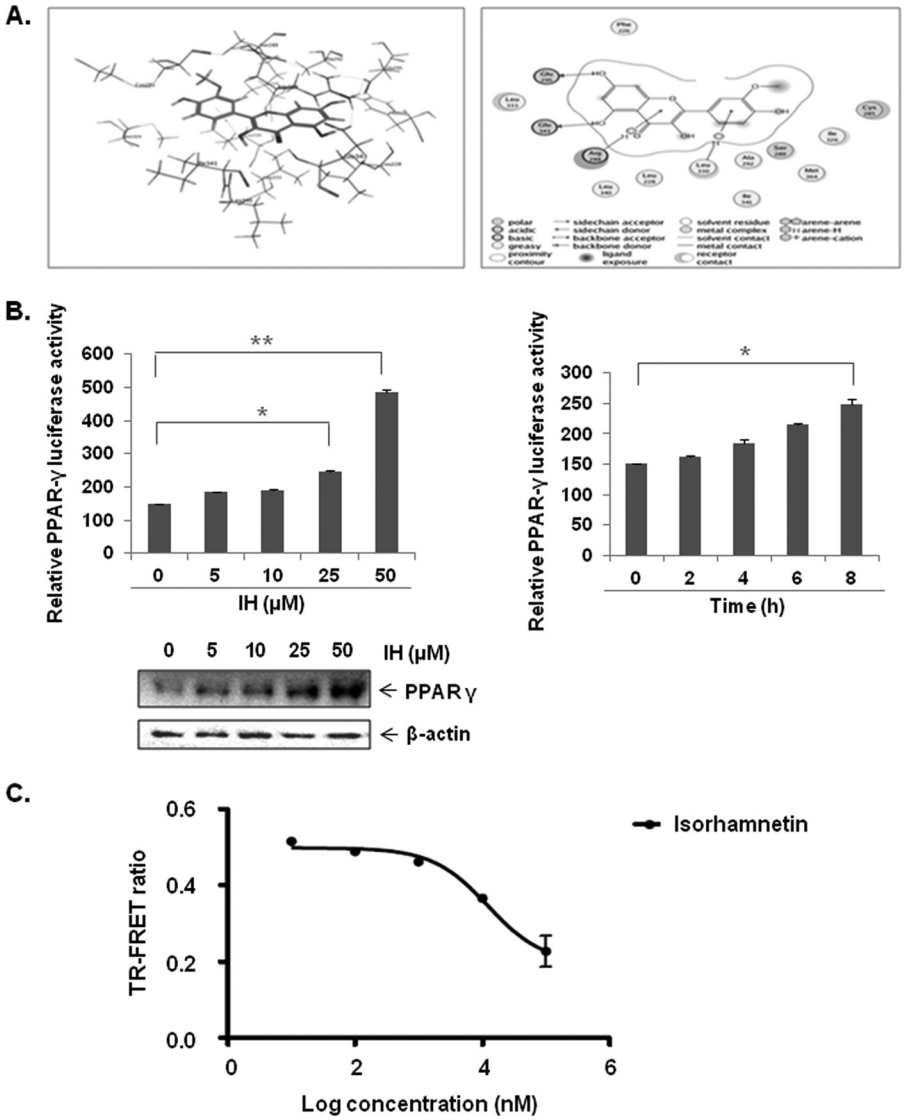

FIGURE 5. *A*, the ligand interaction map of IH inside PPAR-γ (*left panel*) and three-dimensional conformational structure of IH inside PPAR-γ (*right panel*). *B*, IH increases PPAR-γ activity in a dose dependent manner, also shown by Western blot (*left panel*). IH also increases PPAR-γ activity in a time-dependent manner (*right panel*). The cells were transfected with pPPRE-tk-Luc and β-gal plasmid for 4 h before treatment with the indicated concentrations of IH. The data are expressed as percentages of the PPAR-γ activity relative to the control. The values are the means ± S.E. of two or three independent experiments. *, $p < 0.05$; **, $p < 0.01$. *C*, *in vitro* competitive binding assay showed that IH could bind competitively to PPAR-γ. Serial dilutions of IH (1% final Me_2SO concentration, serial dilutions performed in 100% Me_2SO) were prepared in a 384-well polypropylene assay plate. Fluormone™ Pan-PPAR Green, PPAR-γ-LBD, and Tb-anti-GST Ab were then added to each sample well as described in the protocol. The assay mixture was incubated for 1 h at room temperature prior to measuring the 520-nm/490-nm emission ratio of each well. The *error bars* represent the S.E. of duplicate wells ($n = 2$).

duplicate wells ($n = 2$). The results, as shown in Fig. 5*C*, clearly indicate that IH could indeed bind competitively to PPAR-γ with an IC_{50} of 5.98 μM.

GW9662, a Pharmacological PPAR-γ Inhibitor, Reversed the Effect of IH on Apoptosis—We observed above that the antagonist of PPAR-γ, GW9662, could significantly reverse IH-induced PPAR-γ activity (Fig. 4*C*, *left panel*), as well as activity of 15d-PGJ_2, a classical PPAR-γ agonist. (Fig. 4*C*, *right panel*), thereby suggesting that the anticancer effects of IH may be mediated through PPAR-γ pathway. To determine whether the increase in apoptosis was due to IH-induced PPAR-γ activity, GW9662, a pharmacological PPAR-γ inhibitor, was used to block the activation of the PPAR-γ pathway. IH-induced apoptosis was found to be reversed by GW9662, although not completely as observed by annexin V assay (Fig. 6*A*, *left panel*). Transfection efficiency was monitored by Western blot analysis (Fig. 6*A*, *right panel*). These findings suggest that PPAR-γ is involved in IH-induced apoptosis, at least to a partial extent.

Dominant Negative PPAR-γ Impaired the Effect of IH on the PPAR-γ Pathway—The induction of PPAR-γ activity by IH in GC cells was also investigated using a genomic approach. Faulty PPAR-γ nuclear receptor was overexpressed to reduce the possibility of IH binding. It was found that the induction of PPAR-γ activity in AGS cells by IH was significantly reversed in the presence of dominant negative PPAR-γ as observed by luciferase assay results (Fig. 6*B*, *left panel*). Transfection efficiency was monitored by Western blot analysis (Fig. 6*B*, *right panel*).

IH Increases the Expression of PPAR-γ in Gastric Tumor Tissues—We also evaluated the effect of IH on PPAR-γ levels in GC tissue. Fig. 6*C* shows that IH was quite effective in increas-

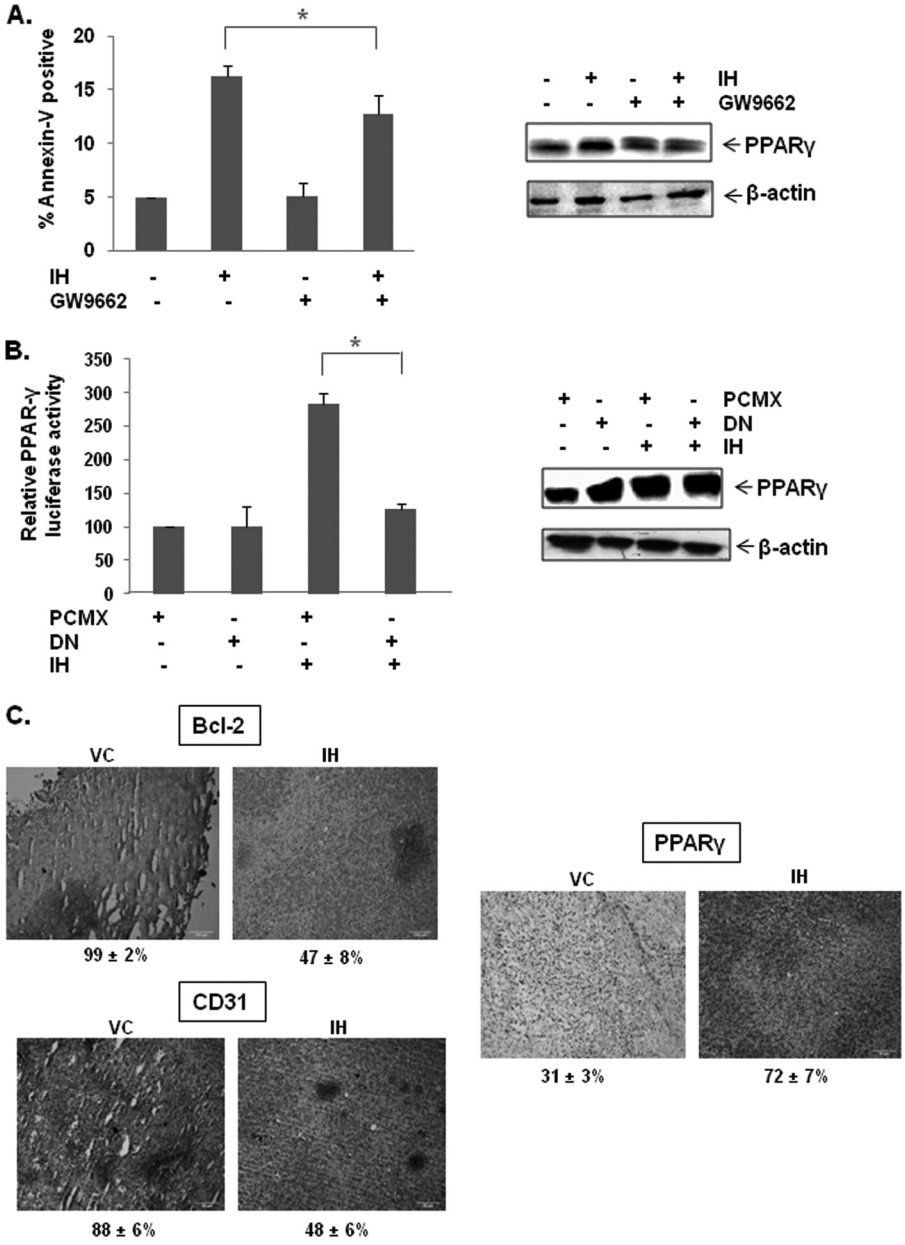

FIGURE 6. **IH-induced PPAR-γ activity could be blocked by GW9662, an inhibitor of PPAR-γ.** *A*, GW9662 partially reverses IH-induced apoptosis in AGS cells tested by annexin V staining. Western blot denotes the efficiency of transfection. The cells were pretreated with 10 or 20 μM of GW9662 for 2 h before treatment with 25 μM of IH for 12 h. The cells were then harvested and stained with annexin V-PI as described under "Experimental Procedures." The values are the means ± S.E. of three independent experiments. *, $p < 0.05$. *B*, dominant negative PPAR-γ reverses IH-induced PPAR-γ activity. Western blot denotes the efficiency of transfection. The cells were transfected with PPAR-γDN or pCMX plasmids, together with pPPRE-tk-Luc and β-gal plasmids for 4 h before treatment with 25 μM of IH for 18 h. The data are expressed as percentages of the PPAR-γ activity relative to the control. The values are means ± S.E. of two or three independent experiments. *, $p < 0.05$. *C*, immunohistochemical analysis of Bcl-2, CD31, and PPAR-γ showed the increase in the expression of PPAR-γ and the inhibition in Bcl-2 and CD31 expression in IH-treated samples as compared with control group. The percentage indicates positive staining for the given biomarker. The photographs were taken at the magnification of 20×.

ing the expression of PPAR-γ in GC tissues. Whether IH can modulate the expression of gene products involved in antiapoptosis (Bcl-2) and angiogenesis (CD31) in GC tissues was also examined. We found that treatment with IH was effective in significantly down-regulating the overexpression of Bcl-2 and CD31 in GC tissue samples (Fig. 6*C*).

DISCUSSION

The aim of this study was to determine whether IH exerts its anticancer effects in GC cells through the modulation of PPAR-γ signaling pathway. We observed that this flavonoid increased PPAR-γ activity and modulated the expression of the PPAR-γ regulated genes in GC cells. Also, the increase in PPAR-γ activity by IH could be reversed in the presence of PPAR-γ pharmacological blocker and a mutated PPAR-γ dominant negative plasmid, thereby indicating that IH can act as a potential novel ligand of PPAR-γ. We further observed that IH could form interactions with seven polar residues and six nonpolar residues within the ligand-binding pocket of PPAR-γ that are reported to be critical for its activity and also competitively

bind to PPAR-γ. IH also caused the inhibition of proliferation, induced apoptosis, as evident by PARP cleavage, and also potentiated the apoptotic effects of chemotherapeutic drugs in GC cells. This hypothesis was also tested in a virtual predictive tumor cell system, and 0.5 and 5 μM with a K_a of 1.19 μM concentrations of IH caused PPAR-γ activation and generated similar biomarker trends as seen experimentally with IH effects on GC cells. Intraperitoneal injection of IH into nude mice bearing subcutaneous SNU-5 xenografts resulted in significant increase in the expression of PPAR-γ and the down-modulation of Bcl-2 and CD31 in treated tumor tissues.

The most important characteristic of a cancer cell remains its ability to sustain proliferation (37). The cellular pathways that control proliferation in normal cells are perturbed in most cancers (38). According to Prof. Weinberg in his classic "Hallmarks of Cancer," tumor cells can proliferate using alternate strategies: autocrine signaling through which they might produce growth factors themselves and respond to it with their own cognate receptors or by manipulating normal cells in providing them with growth factors (39). Thus, we first analyzed the effect of IH on the proliferation of GC cells. Our results clearly showed that IH could indeed inhibit the proliferation of three GC cell lines, (AGS, SNU5, and MKN45) in a dose- and time-dependent manner. It is interesting to note that though IH could inhibit the proliferation of various GC cells; it showed minimal effect on the proliferation of normal GC cells, thereby indicating that it is not substantially cytotoxic to normal cells. We also show for the first time that IH can enhance the cytotoxic effects of chemotherapeutic agents commonly employed in GC treatment. Together, these results suggest that IH can be used as a complement to conventional chemotherapeutic drugs for the purpose of enhancing the antitumor effect and/or reducing toxicity of the latter. To understand the mechanism of how IH exerts its growth inhibitory effects, we evaluated its effect on the apoptosis in GC cells. We found that IH was able to induce significant apoptosis concomitant with down-regulation in the expression of the various antiapoptotic/antiproliferative proteins (Bcl-2, Bcl-xL, and Cyclin-D1), caused an increase in the expression of procaspase-9/3, and caused PARP cleavage in a time-dependent manner in GC cells.

Cancer metastasis refers to the spread of cancer cells from the primary neoplasm to distant sites, where secondary tumors are formed, and is considered one of the major causes of cancer mortality (40–42). Therefore, we also analyzed the effect of IH on the GC migration and invasion, and our study is the first to demonstrate that IH could inhibit the migratory and invasive properties of GC cells. These effects could also be reversed in the presence of a pharmacological PPAR-γ inhibitor, thereby indicating that the antimigratory/invasive effects of IH may be mediated through the activation of PPAR-γ signaling pathway.

Next, we decided to elucidate the molecular mechanisms underlying the observed anticancer effects of IH and investigated its effect on the activation of PPAR-γ, a nuclear receptor reported to play an important role in the initiation and development of GC (43). In a study to elucidate the role of PPAR-γ in GC, it was found that the loss of the receptor promoted gastric carcinogenesis (17). PPAR-γ has been reported to be expressed in high levels in GC, and it was shown that activated PPAR-γ could induce apoptosis in GC cells (45). In our study, we found that IH could physically interact with PPAR-γ at five polar residues and nine nonpolar residues, of which two interactions, Cys-285 and Ser-289, were previously found to be important for its binding and activity (44, 46, 47). We also observed that IH can activate PPAR-γ in a time- and dose-dependent manner and can competitively bind to the receptor with increasing concentrations. Interestingly, IH-induced apoptosis could be inhibited by PPAR-γ antagonist, GW9662, thereby indicating that the anticancer effects of IH may be mediated through the PPAR-γ activation pathway. The results obtained from the virtual technology platform also supported our hypothesis that IH could indeed activate PPAR-γ and could modulate various gene products involved in proliferation, survival, and metastasis of GC.

Whether these *in vitro* observations with IH have any relevance under *in vivo* settings was also investigated. Our results also indicate for the first time that IH can indeed significantly increase the expression of PPAR-γ and down-regulate the expression Bcl-2 and CD31 in treated tumor tissues as compared with control group. To the best of our knowledge, no prior studies with IH in xenograft GC models have been reported so far, and our overall findings suggest that IH has a tremendous potential for the treatment of GC. IH has been reported to exhibit significant anti-inflammatory, antiproliferative, pro-apoptotic, and chemopreventive effects in selected tumor cells and mice models. However, it has never been tested in humans before, and hence its clinically relevant doses are not known as yet. Further studies in humans are required before its clinical potential is fully realized in cancer treatment. Thus, overall, our experimental and predictive experiment results clearly indicate that antiproliferative and pro-apoptotic effects of IH in GC are mediated through activation of PPAR-γ and provide a sound basis for pursuing the use of IH further, either alone or in combination with existing therapy, to reduce the side effects and enhance treatment efficacy for GC.

REFERENCES

1. Ford, A. C. (2011) Chemoprevention for gastric cancer. *Best Pract. Res. Clin. Gastroenterol.* **25,** 581–592
2. Yeoh, K. G. (2007) How do we improve outcomes for gastric cancer? *J. Gastroenterol. Hepatol.* **22,** 970–972
3. Lochhead, P., and El-Omar, E. M. (2008) Gastric cancer. *Br. Med. Bull.* **85,** 87–100
4. Roukos, D. H., and Kappas, A. M. (2005) Perspectives in the treatment of gastric cancer. *Nat. Clin. Pract. Oncol.* **2,** 98–107
5. Ohtsu, A. (2008) Chemotherapy for metastatic gastric cancer. Past, present, and future. *Journal of gastroenterology* **43,** 256–264
6. Selgrad, M., Bornschein, J., Rokkas, T., and Malfertheiner, P. (2010) Clinical aspects of gastric cancer and *Helicobacter pylori*. Screening, prevention, and treatment. *Helicobacter* **15,** 40–45
7. Koeffler, H. P. (2003) Peroxisome proliferator-activated receptor γ and cancers. *Clin. Cancer Res.* **9,** 1–9
8. Bishop-Bailey, D. (2011) PPARs and angiogenesis. *Biochem. Soc. Trans.* **39,** 1601–1605
9. Peters, J. M., Shah, Y. M., and Gonzalez, F. J. (2012) The role of peroxisome proliferator-activated receptors in carcinogenesis and chemoprevention. *Nat. Rev. Cancer* **12,** 181–195
10. Wang, T., Xu, J., Yu, X., Yang, R., and Han, Z. C. (2006) Peroxisome proliferator-activated receptor γ in malignant diseases. *Crit. Rev. Oncol. Hematol.* **58,** 1–14
11. Schmidt, M. V., Brune, B., and von Knethen, A. (2010) The nuclear hor-

mone receptor PPARγ as a therapeutic target in major diseases. *Sci. World J.* **10,** 2181–2197
12. Mannelli, M., Cantini, G., Poli, G., Mangoni, M., Nesi, G., Canu, L., Rapizzi, E., Borgogni, E., Ercolino, T., Piccini, V., and Luconi, M. (2010) Role of the PPAR-γ system in normal and tumoral pituitary corticotropic cells and adrenal cells. *Neuroendocrinology* **92,** 23–27
13. Wan, Z., Shi, W., Shao, B., Shi, J., Shen, A., Ma, Y., Chen, J., and Lan, Q. (2011) Peroxisome proliferator-activated receptor γ agonist pioglitazone inhibits β-catenin-mediated glioma cell growth and invasion. *Mol. Cell. Biochem.* **349,** 1–10
14. Kumar, A. P., Quake, A. L., Chang, M. K., Zhou, T., Lim, K. S., Singh, R., Hewitt, R. E., Salto-Tellez, M., Pervaiz, S., and Clément, M. V. (2009) Repression of NHE1 expression by PPARγ activation is a potential new approach for specific inhibition of the growth of tumor cells in vitro and in vivo. *Cancer Res.* **69,** 8636–8644
15. Yokoyama, Y., Xin, B., Shigeto, T., and Mizunuma, H. (2011) Combination of ciglitazone, a peroxisome proliferator-activated receptor γ ligand, and cisplatin enhances the inhibition of growth of human ovarian cancers. *J. Cancer Res. Clin. Oncol.* **137,** 1219–1228
16. Yao, L., Liu, F., Sun, L., Wu, H., Guo, C., Liang, S., Liu, L., Liu, N., Han, Z., Zhang, H., Wu, K., and Fan, D. (2010) Upregulation of PPARγ in tissue with gastric carcinoma. *Hybridoma* **29,** 341–343
17. Lu, J., Imamura, K., Nomura, S., Mafune, K., Nakajima, A., Kadowaki, T., Kubota, N., Terauchi, Y., Ishii, G., Ochiai, A., Esumi, H., and Kaminishi, M. (2005) Chemopreventive effect of peroxisome proliferator-activated receptor γ on gastric carcinogenesis in mice. *Cancer Res.* **65,** 4769–4774
18. Reka, A. K., Goswami, M. T., Krishnapuram, R., Standiford, T. J., and Keshamouni, V. G. (2011) Molecular cross-regulation between PPAR-γ and other signaling pathways. Implications for lung cancer therapy. *Lung Cancer* **72,** 154–159
19. Nickkho-Amiry, M., McVey, R., and Holland, C. (2012) Peroxisome proliferator-activated receptors modulate proliferation and angiogenesis in human endometrial carcinoma. *Mol. Cancer Res.* **10,** 441–453
20. Papi, A., Rocchi, P., Ferreri, A. M., and Orlandi, M. (2010) RXRγ and PPARγ ligands in combination to inhibit proliferation and invasiveness in colon cancer cells. *Cancer Lett.* **297,** 65–74
21. Oyekan, A. (2011) PPARs and their effects on the cardiovascular system. *Clin. Exp. Hypertension* **33,** 287–293
22. Wilding, J. P. (2012) PPAR agonists for the treatment of cardiovascular disease in patients with diabetes. *Diabetes Obes. Metab.*, in press
23. Chen, Y. C., Wu, J. S., Tsai, H. D., Huang, C. Y., Chen, J. J., Sun, G. Y., and Lin, T. N. (2012) Peroxisome proliferator-activated receptor gamma (PPAR-γ) and neurodegenerative disorders. *Mol. Neurobiol.* **46,** 114–124
24. Yao, H., Xu, W., Shi, X., and Zhang, Z. (2011) Dietary flavonoids as cancer prevention agents. *J. Environ. Sci. Health C Environ. Carcinog. Ecotoxicol. Rev.* **29,** 1–31
25. Asensi, M., Ortega, A., Mena, S., Feddi, F., and Estrela, J. M. (2011) Natural polyphenols in cancer therapy. *Crit. Rev. Clin. Lab. Sci.* **48,** 197–216
26. Cushnie, T. P., and Lamb, A. J. (2011) Recent advances in understanding the antibacterial properties of flavonoids. *Int. J. Antimicrob. Agents* **38,** 99–107
27. Wang, P., Heber, D., and Henning, S. M. (2012) Quercetin increased the antiproliferative activity of green tea polyphenol (−)-epigallocatechin gallate in prostate cancer cells. *Nutr. Cancer* **64,** 580–587
28. Wang, P., Zhang, K., Zhang, Q., Mei, J., Chen, C. J., Feng, Z. Z., and Yu, D. H. (2012) Effects of quercetin on the apoptosis of the human gastric carcinoma cells. *Toxicol. In Vitro* **26,** 221–228
29. Jaramillo, S., Lopez, S., Varela, L. M., Rodriguez-Arcos, R., Jimenez, A., Abia, R., Guillen, R., and Muriana, F. J. (2010) The flavonol isorhamnetin exhibits cytotoxic effects on human colon cancer cells. *J. Agric. Food Chem.* **58,** 10869–10875
30. Kim, J. E., Lee, D. E., Lee, K. W., Son, J. E., Seo, S. K., Li, J., Jung, S. K., Heo, Y. S., Mottamal, M., Bode, A. M., Dong, Z., and Lee, H. J. (2011) Isorhamnetin suppresses skin cancer through direct inhibition of MEK1 and PI3-K. *Cancer Prev. Res.* **4,** 582–591
31. Lee, H. J., Lee, H. J., Lee, E. O., Ko, S. G., Bae, H. S., Kim, C. H., Ahn, K. S., Lu, J., and Kim, S. H. (2008) Mitochondria-cytochrome C-caspase-9 cascade mediates isorhamnetin-induced apoptosis. *Cancer Lett.* **270,** 342–353
32. Choi, K. C., Chung, W. T., Kwon, J. K., Yu, J. Y., Jang, Y. S., Park, S. M., Lee, S. Y., and Lee, J. C. (2010) Inhibitory effects of quercetin on aflatoxin B1-induced hepatic damage in mice. *Food Chem. Toxicol.* **48,** 2747–2753
33. Woo, C. C., Loo, S. Y., Gee, V., Yap, C. W., Sethi, G., Kumar, A. P., and Tan, K. H. (2011) Anticancer activity of thymoquinone in breast cancer cells. Possible involvement of PPAR-γ pathway. *Biochem. Pharmacol.* **82,** 464–475
34. Kannaiyan, R., Hay, H. S., Rajendran, P., Li, F., Shanmugam, M. K., Vali, S., Abbasi, T., Kapoor, S., Sharma, A., Kumar, A. P., Chng, W. J., and Sethi, G. (2011) Celastrol inhibits proliferation and induces chemosensitization through down-regulation of NF-κB and STAT3 regulated gene products in multiple myeloma cells. *Br. J. Pharmacol.* **164,** 1506–1521
35. Manu, K. A., Shanmugam, M. K., Rajendran, P., Li, F., Ramachandran, L., Hay, H. S., Kannaiyan, R., Swamy, S. N., Vali, S., Kapoor, S., Ramesh, B., Bist, P., Koay, E. S., Lim, L. H., Ahn, K. S., Kumar, A. P., and Sethi, G. (2011) Plumbagin inhibits invasion and migration of breast and gastric cancer cells by downregulating the expression of chemokine receptor CXCR4. *Mol. Cancer* **10,** 107
36. Shanmugam, M. K., Rajendran, P., Li, F., Nema, T., Vali, S., Abbasi, T., Kapoor, S., Sharma, A., Kumar, A. P., Ho, P. C., Hui, K. M., and Sethi, G. (2011) Ursolic acid inhibits multiple cell survival pathways leading to suppression of growth of prostate cancer xenograft in nude mice. *J. Mol. Med.* **89,** 713–727
37. Kelly, P. N., and Strasser, A. (2011) The role of Bcl-2 and its pro-survival relatives in tumourigenesis and cancer therapy. *Cell Death Differ.* **18,** 1414–1424
38. Evan, G. I., and Vousden, K. H. (2001) Proliferation, cell cycle and apoptosis in cancer. *Nature* **411,** 342–348
39. Hanahan, D., and Weinberg, R. A. (2011) Hallmarks of cancer. The next generation. *Cell* **144,** 646–674
40. Carmeliet, P., and Jain, R. K. (2011) Molecular mechanisms and clinical applications of angiogenesis. *Nature* **473,** 298–307
41. Patel, L. R., Camacho, D. F., Shiozawa, Y., Pienta, K. J., and Taichman, R. S. (2011) Mechanisms of cancer cell metastasis to the bone. A multistep process. *Future Oncol.* **7,** 1285–1297
42. Hannelien, V., Karel, G., Jo, V. D., and Sofie, S. (2012) The role of CXC chemokines in the transition of chronic inflammation to esophageal and gastric cancer. *Biochim. Biophys. Acta* **1825,** 117–129
43. Burris, T. P., Busby, S. A., and Griffin, P. R. (2012) Targeting orphan nuclear receptors for treatment of metabolic diseases and autoimmunity. *Chem. Biol.* **19,** 51–59
44. Nolte, R. T., Wisely, G. B., Westin, S., Cobb, J. E., Lambert, M. H., Kurokawa, R., Rosenfeld, M. G., Willson, T. M., Glass, C. K., and Milburn, M. V. (1998) Ligand binding and co-activator assembly of the peroxisome proliferator-activated receptor-γ. *Nature* **395,** 137–143
45. Takahashi, N., Okumura, T., Motomura, W., Fujimoto, Y., Kawabata, I., and Kohgo, Y. (1999) Activation of PPARγ inhibits cell growth and induces apoptosis in human gastric cancer cells. *FEBS Lett.* **455,** 135–139
46. Boik, J. C., and Newman, R. A. (2008) A classification model to predict synergism/antagonism of cytotoxic mixtures using protein-drug docking scores. *BMC Pharmacol.* **8,** 13
47. Salam, N. K., Huang, T. H., Kota, B. P., Kim, M. S., Li, Y., and Hibbs, D. E. (2008) Novel PPAR-γ agonists identified from a natural product library. A virtual screening, induced-fit docking and biological assay study. *Chem. Biol. Drug Des.* **71,** 57–70